

Salt Dependent Stability of Stearic Acid Langmuir-Blodgett Films Exposed to Aqueous Electrolytes

Naveen Kumar, Lei Wang, Igor Siretanu, Michael H.G. Duits, and Frieder Mugele

Langmuir, Just Accepted Manuscript • DOI: 10.1021/la400615j • Publication Date (Web): 08 Apr 2013

Downloaded from <http://pubs.acs.org> on April 19, 2013

Just Accepted

“Just Accepted” manuscripts have been peer-reviewed and accepted for publication. They are posted online prior to technical editing, formatting for publication and author proofing. The American Chemical Society provides “Just Accepted” as a free service to the research community to expedite the dissemination of scientific material as soon as possible after acceptance. “Just Accepted” manuscripts appear in full in PDF format accompanied by an HTML abstract. “Just Accepted” manuscripts have been fully peer reviewed, but should not be considered the official version of record. They are accessible to all readers and citable by the Digital Object Identifier (DOI®). “Just Accepted” is an optional service offered to authors. Therefore, the “Just Accepted” Web site may not include all articles that will be published in the journal. After a manuscript is technically edited and formatted, it will be removed from the “Just Accepted” Web site and published as an ASAP article. Note that technical editing may introduce minor changes to the manuscript text and/or graphics which could affect content, and all legal disclaimers and ethical guidelines that apply to the journal pertain. ACS cannot be held responsible for errors or consequences arising from the use of information contained in these “Just Accepted” manuscripts.



Salt Dependent Stability of Stearic Acid Langmuir-Blodgett Films Exposed to Aqueous Electrolytes

Naveen Kumar¹, Lei Wang¹, Igor Siretanu, Michel Duits, and Frieder Mugele*

Physics of Complex Fluids Group and MESA+ Institute, Faculty of Science and Technology, University of Twente, PO Box 217, 7500 AE Enschede, The Netherlands

ABSTRACT

We use contact angle goniometry, imaging ellipsometry and atomic force microscopy to study the stability and wettability of Langmuir-Blodgett (LB) monolayers of stearic acid on silica substrates, upon drying and exposure to aqueous solutions of varying salinity. The influences of Ca^{2+} and Na^+ ions are compared by varying their concentrations, both in the subphase before the LB transfer, and in the droplets to which the dried LB layers are exposed. Ca^{2+} ions in the subphase are found to enhance the stability, leading to contact angles up to 100 degrees, as compared to less than 5 degrees for Na^+ . Consistent with the macroscopic wettability, AFM images show almost intact films with few holes exposing bare substrate when prepared in presence of Ca^{2+} while subphases containing Na^+ result in large areas of bare substrate after exposure to aqueous drops. The observations on varying the composition of the droplets corroborate the stabilizing effect of Ca^{2+} . We attribute these findings to the cation-bridging ability of Ca^{2+} ions, which can bind the negatively charged stearate groups to the negatively charged substrates. We discuss the relevance of our findings in the context of enhanced oil recovery.

¹ N.K. and L.W. contributed equally to the present work.

* To whom correspondence should be addressed. E-mail: f.mugele@utwente.nl

Introduction

The interaction of organic matter with solid surfaces in an ambient aqueous environment plays a key role in many processes and phenomena in nature, science, and technology including ground water-soil interaction, water purification, lubrication, corrosion inhibition, colloidal stability, Langmuir Blodgett (LB) films, (membrane) fouling, and enhanced oil recovery.¹⁻⁵ Two processes are crucial: the binding of the amphiphilic molecules to the substrate, and their assembly into an interfacial layer.

Since most solid surfaces, including in particular mineral and glass surfaces, assume a finite surface charge in water, usually electrostatic effects contribute strongly to the interactions with polar and/or charged organic molecules. Divalent ions as well as higher multivalent ions are known to be particularly efficient ‘glues’ that stick organic molecules to solid surfaces.⁵⁻⁶ For instance, biophysicists make extensive use of this mechanism to immobilize DNA and proteins onto solid surfaces, for example to enable their visualization by Atomic Force Microscopy.⁷ Monovalent ions, in contrast, are unable to provide such strong immobilization.

Additionally, organic films can also undergo rearrangements in three dimensions when they are exposed to aqueous solutions of multivalent ions. It has been reported that mobile counterions⁸⁻¹⁰ embedded into layers of fatty acids can trigger structural rearrangements of molecules. A particularly dramatic example involves a so called ‘flip-over’, in which the molecules form a bilayer which exposes the polar head groups to the substrate and to the aqueous phase.¹¹⁻¹²

Both (un)binding events and rearrangements can have a tremendous influence on the chemical affinity of the surface that is exposed to the aqueous liquid: the difference between

1
2
3 hydrophilic and charged (for bare substrate), and hydrophobic (for coated substrates) gives
4
5 rise to a completely different water wettability. Also the interactions between two such
6
7 surfaces immersed in water change: from DLVO-type for the bare surfaces, to long-range
8
9 attractive in case of some hydrophobized surfaces.^{11, 13-16} In the present study we focus on the
10
11 question, how the wettability of an adsorbed organic layer can be changed via exposure to
12
13 aqueous solutions with different overall salinity and ionic compositions. While this is of
14
15 interest for many applications (as indicated), the present paper is inspired in particular by
16
17 recent observations in the field of enhanced oil recovery (EOR).
18
19

20
21 In traditional (i.e. secondary) oil recovery, highly saline seawater is pumped into the
22
23 ground to expel oil from pores in the rock.^{5,17} However this process is not very efficient.
24
25 Evidence has been growing that reducing the overall salinity (and in particular the concen-
26
27 tration of divalent ions) of the injected water can substantially increase the oil recovery rate.^{5,}
28
29 ¹⁷ A possible explanation of this observation assumes that over geological time scales, the
30
31 intrinsically hydrophilic rock was turned into hydrophobic via the adsorption of polar
32
33 components from the crude oil. In this picture, the hydrophobic layers become bound (at least
34
35 partly) via electrostatic interactions. In particular multivalent ions like Ca^{2+} and Mg^{2+} are
36
37 supposed to play a role, since these can bind acid groups from the oil to negatively charged
38
39 sites on the surface via an ion bridging mechanism.
40
41
42
43
44

45 The effectiveness of using low salinity water then lies in weakening the bonding
46
47 between the hydrophobic layers and the rock. As a consequence, the organic layers can be
48
49 (partially) released. This renders the rock more hydrophilic, and facilitates the expulsion of oil
50
51 from the narrow pores via a reduction in the required Laplace pressure. Ultimately this would
52
53 explain the increased efficiency of the oil recovery process. Since the characteristic flow rates
54
55 in oil recovery are of order one foot per day, corresponding to approximately $1 \mu\text{m/s}$, the
56
57
58
59
60

1
2
3 decomposition of the hydrophobic layers should take place on much shorter time scales that
4
5 are much more accessible in the laboratory.
6
7

8
9 The purpose of the present study is to develop a model system and to test various
10 aspects of the scenario described above. In particular, we want to correlate macroscopic
11 variations of the wettability with the microscopic decomposition or rearrangement of the
12 hydrophobic layers and elucidate the relevance of divalent ions in this process. To this end,
13 we choose one of the best characterized model systems of thin organic layers, namely
14 monolayers of stearic acid (SA) that we deposit onto solid surfaces using the Langmuir
15 Blodgett (LB) technique. While the details of this deposition are of course very different
16 compared to the gradual adsorption from crude oil, LB transfer offers unique control of the
17 physico-chemical parameters that govern the stability of the resulting film.
18
19
20
21
22
23
24
25
26
27
28

29 Monolayers of SA and other fatty acids have been investigated in great detail in the
30 past, both as Langmuir layers at the air-water interface¹⁸⁻²⁰ and as LB films deposited onto
31 solid surfaces^{12, 21} dating back all the way to the original work of Blodgett²² and Langmuir.²³
32
33 It is well known that both the physical and chemical properties of such layers depend very
34 much on pH and on the ion content of an adjacent aqueous phase.²⁴⁻²⁵ A summary of early
35 work based to an important extent on surface potential measurements has been summarized
36 by Goddard.²⁶ At low pH, the carboxylic acid groups and solid surfaces like silica remain
37 protonated and the affinity to ions (and interfaces) is weak. In contrast, at high pH, they are
38 deprotonated and interact strongly with the ions.^{8, 25, 27-28} This affects amongst other things the
39 transferability of Langmuir monolayers in the LB process^{10, 29} and the stability of the layers.²⁵
40
41 More recently, Graber et al.³⁰ studied the consequences of these ideas for the macroscopic
42 water-repellency of soils hydrophobized by fatty acids upon exposure to water of variable pH
43 and salt contents. They demonstrated that such soils indeed resist the penetration of water
44
45
46
47
48
49
50
51
52
53
54
55
56
57
58
59
60

1
2
3 drops more efficiently upon increasing the pH and calcium concentration. The mechanisms
4
5 invoked to explain these observations are very similar to the proposed mechanism of
6
7 enhanced oil recovery by low salinity water flooding. All these previous observations suggest
8
9 that SA is a suitable model compound for our purpose.
10

11
12 In this work, we study the influence of Ca^{2+} and Na^+ ions on the stability and wettability
13
14 of stearic acid monolayers. The layers are deposited onto oxidized silicon wafers mimicking
15
16 silica surfaces using LB transfer. Subsequently we expose the surfaces to drops of variable
17
18 salinity. Occasionally, mica is used as an alternative substrate representing clays. We
19
20 investigate the effect of ions on the film stability in two complementary ways. First, we vary
21
22 the ion contents of the subphase during LB transfer. Second, we vary the ion contents of the
23
24 aqueous phase to which the LB films are exposed after the transfer. In both cases we focus on
25
26 Na^+ and Ca^{2+} ions representing the prevalent mono- and divalent cations of sea water,
27
28 respectively. Macroscopic contact angle goniometry, imaging ellipsometry, and Atomic Force
29
30 Microscopy (AFM) consistently show that Ca^{2+} has a pronounced stabilizing effect on the SA
31
32 films exposed to water. Microscopic AFM images demonstrate the partial decomposition of
33
34 the LB films upon exposure to water. In the absence of multilayer formation, the contact angle
35
36 of sessile drops on partially decomposed LB films is found to agree with the expectations
37
38 based on the AFM data using Cassie's equation.
39
40
41
42
43
44

45 **MATERIALS AND METHODS**

46 **Chemicals and solutions:**

47
48
49 All solvents and reagents are obtained from Sigma-Aldrich and used without further
50
51 purification. Solution of stearic acid (SA) (octadecanoic acid, $\text{CH}_3(\text{CH}_2)_{16}\text{COOH}$, grade 1,
52
53 approx. 99%) is prepared in chloroform (CHCl_3 , ACS reagent) at a concentration of 1 mg/mL.
54
55
56
57
58
59
60

1
2
3 Aqueous subphases for the LB-transfer are prepared by dissolving sodium chloride (NaCl)
4 and/or calcium chloride dihydrate ($\text{CaCl}_2 \cdot 2\text{H}_2\text{O}$) (both ACS reagent grade) in deionized water
5 (Synergy UV, Millipore, resistance 18.2 $\text{M}\Omega \cdot \text{cm}$). Three different types of subphases are used
6
7 containing 0.5 M NaCl, 0.01 M CaCl_2 , and a mixture of 0.5 M NaCl, and 0.01 M CaCl_2 ,
8
9 respectively. These values of concentrations are chosen to mimic typical concentrations in sea
10
11 water as it is used in secondary oil recovery. In all cases, the pH of these subphases is
12
13 adjusted to 9.5 ± 0.1 with 0.1 M standard solution of NaOH, to ensure that the carboxylic acid
14
15 groups of stearic acid are largely deprotonated²⁴ and to prevent substantial dissolution of
16
17 stearate molecules in the bulk water, which occurs for $\text{pH} > 10$.²⁸
18
19
20
21
22
23

24 **Substrate preparation and LB film deposition:**

25
26
27 As substrates, we use commercial silicon (100) wafers with a thermally grown oxide
28
29 layer of ~ 35 nm thickness. The wafers are cut into pieces of 1×5 cm^2 . The substrates are
30
31 cleaned by the following procedure: firstly, samples were extensively rinsed with successively
32
33 Millipore water, iso-propanol, and ethanol, then gently dried with N_2 gas; secondly, wafers
34
35 were exposed to ambient air plasma (PDC-32G-2, Harrick plasma) for 30-40 min. This
36
37 procedure assures good hydrophilicity of the substrate (water contact angle: $\theta < 5^\circ$). AFM is
38
39 used to verify the smoothness of the substrate. The typical RMS (root means square)
40
41 roughness is found to be < 0.2 nm.
42
43
44

45
46 LB film deposition is performed using a computer-controlled trough from Nima
47
48 Technology. Prior to the experiment, the trough is rigorously cleaned with pure water, ethanol
49
50 and chloroform. The system is assumed to be clean if the surface pressure of the bare
51
52 subphase (*i.e.* prior to spreading the SA solution) varies by no more than 0.1 mN/m upon
53
54 moving the barriers back and forth. Subsequently, a drop (50 μL) of the SA solution in
55
56 chloroform is deposited on the subphase. Around 30 min are allowed for the solvent to
57
58
59
60

1
2
3 evaporate and for the SA layer to spread before initiating the LB transfer. All LB transfers are
4
5 performed at a constant surface pressure of 30 mN/m, just above the kink in the pressure-area
6
7 isotherm that indicates the apparition of a compact solidified layer (see Fig. 1). The pulling
8
9 speed is 2 mm/min. Under these conditions, the transfer ratio for the monolayers is unity
10
11 implying that the substrates become completely covered by the monolayers. Qualitatively
12
13 similar results were obtained in a few test measurements at a somewhat higher transfer
14
15 pressure (45 mN/m).
16
17
18

19
20 In the following, we denote the LB layers transferred with the three different types of
21
22 subphases as SA-Na, SA-Ca, and SA-Ca+Na films, respectively, to indicate the type of cation
23
24 present during the transfer. Before further characterization using contact angle goniometry,
25
26 ellipsometry and AFM, the samples are stored in a glove box under a continuous flow of dry
27
28 nitrogen for 20 hours. All experiments are performed within 2-3 days of preparation.
29
30

31 **Contact angle measurements:**

32
33
34 An optical contact angle goniometer with automated data analysis software (OCA 20L;
35
36 Dataphysics) is used to assess the macroscopic wettability and to determine static water
37
38 contact angles on the samples with measurement accuracy of $\pm 0.5^\circ$. Droplets of 5–10 μL of
39
40 pure water or saline solutions are placed on the surfaces in ambient environment. Goniometry
41
42 measurements are performed after 20 hours of sample preparation at least at 3-4 different
43
44 locations on each sample. For any given sample the contact angle values are reproducible
45
46 within $\pm 3^\circ$.
47
48
49

50 **Ellipsometry imaging:**

51
52
53 The morphology of the transferred monolayers is analyzed after drying using an
54
55 imaging ellipsometer at a wavelength of 658 nm (EP3 Nanoscope, Accurion). Absolute
56
57
58
59
60

1
2
3 thickness maps of the material are obtained by measuring the ellipsometric angles ψ and Δ as
4
5 a function of the position on the substrate, and using the (complex) refractive indices n_i of
6
7 both layer and substrate along with the Fresnel equations to translate (ψ , Δ) into a thickness
8
9 d_i .³¹ Fitting ψ and Δ for the bare substrate with a two-layer model (Si: $d \rightarrow \infty$, $n_{\text{Si}} = 3.96 - 0.02i$
10
11 and SiO_2 : $n_{\text{SiO}_2} = 1.5$) yields the exact value of the oxide thickness (with precision of 0.1 nm).
12
13 The thickness of the transferred SA layers is then calculated using a three-layer model using
14
15 the previously determined oxide thickness as a fixed input and assuming a refractive index of
16
17 $n_{\text{SA}} = 1.43$ for SA.
18
19

20 21 **AFM imaging:**

22
23
24 The topography of treated and untreated SA layers on the nanometer scale is obtained
25
26 under ambient conditions (unless otherwise noted) with a commercial atomic force
27
28 microscope (Dimension Icon AFM with Nanoscope V controller, Bruker AXS). All images
29
30 are collected in tapping mode with ScanAsyst Air and ScanAsyst fluid silicon probes
31
32 purchased from Bruker with sharp tips. Nominal cantilever and tip properties are as follows:
33
34 tip radius < 10 nm; tip height, $0.5 - 0.75$ μm ; cantilever spring constant 0.4 N/m. The AFM is
35
36 operated under “gentle” conditions with small cantilever oscillation amplitudes (< 10 nm) and
37
38 weak damping (i.e. high amplitude setpoint values) to protect both tip and sample against
39
40 damage. Around 3-4 topography and phase images are recorded at representative
41
42 neighbouring locations on each surface. Image analysis is performed using Bruker’s standard
43
44 Nanoscope Analysis 1.4 package.
45
46
47
48

49 50 **Monolayer characterization:**

51
52
53 Initial images of the SA layers after preparation and drying show a flat topography
54
55 with both AFM and ellipsometry in ambient air under all preparation conditions. Inset Fig. 1b
56
57
58
59
60

shows a representative AFM image with a typical roughness of approximately 0.15 nm rms. The Fig. 1c and 1d show the typical ellipsometry thickness map and profile. The observed average thickness of ~ 2 nm is consistent with the length of SA molecules and thus with the expected molecular structure as sketched in the inset Fig. 1a'.³² Yet, the topography, thickness and roughness of these monolayers highly depend on details of sample cleaning, preparation and drying protocols. For the non-optimized conditions, the monolayer could also have some holes in it or dirt sticks to it just after the preparation (supporting information). We have discarded all such monolayers from further analysis in the present study.

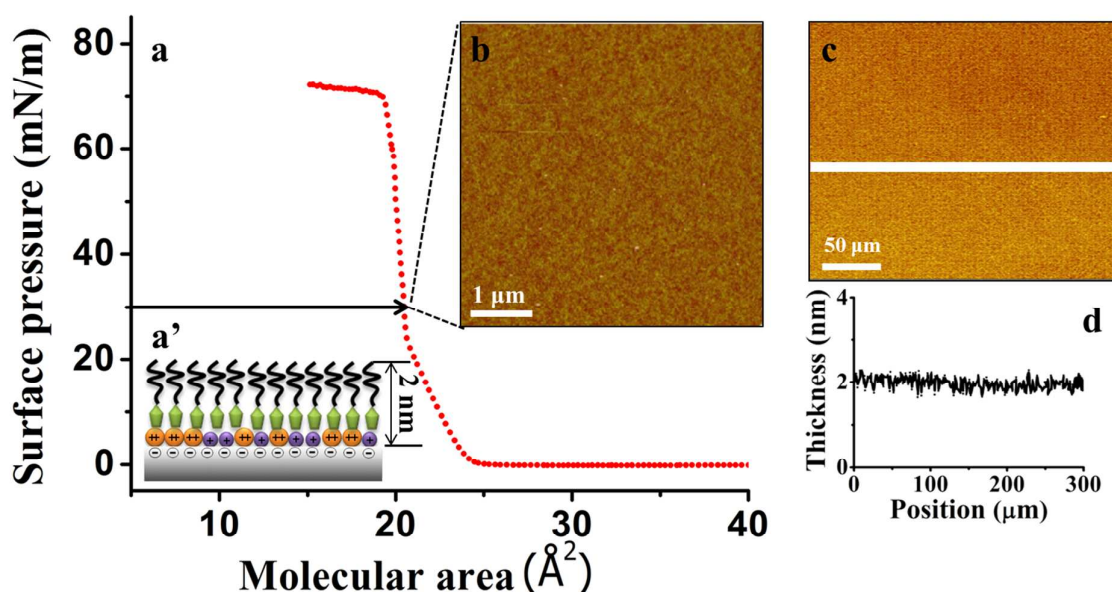


Figure 1. (a) Surface pressure versus area (π -A) isotherm of stearic acid with 0.5 M NaCl aqueous subphase. (a') Schematic illustration of deposited monolayer (b) AFM image (c) Ellipsometry thickness map and (d) corresponding profile of a SA-Na monolayer.

RESULTS

To study the stability of the SA monolayers, we expose all layers to drops of an aqueous “exposure” solution with variable concentrations of NaCl and CaCl₂ at pH ~ 6 . Drops with a

1
2
3 volume of 10 μL are deposited onto the substrates and left there for a period of 10 min.
4
5 During this period we continuously monitor the contact angle. Subsequently the drops are
6
7 removed from the substrate and the samples are blown dry using dry nitrogen. AFM and
8
9 ellipsometry images are recorded both in the center and at the edge of the region previously
10
11 covered by the drops. We discuss first the influence of the composition of the subphase on the
12
13 layer stability upon exposure to pure water and subsequently, the effect of various salts added
14
15 to the drop destabilizing the film.
16
17

18 19 **1. Influence of the subphase composition**

20
21
22 The contact angle θ of the (pure) water drop is found to decrease from an initial value θ_0
23
24 to a significantly smaller equilibrium value θ_e within a few seconds. The latter value is stable
25
26 for several minutes until it begins to decrease slowly due to evaporation. This qualitative
27
28 behavior is similar for all samples. The absolute values of θ_0 are difficult to determine due to
29
30 the limited time resolution of the data acquisition and due to inertial effects that are known to
31
32 affect the drop dynamics within the first fraction of a second of contact.³³ For the present
33
34 study, however, the quantity of interest is the limiting contact angle θ_e at long time scales.
35
36
37

38
39 As shown in Fig. 2, θ_e depends very strongly on the composition of the subphase and
40
41 decreases from approximately 80° for SA-Ca layers to $\sim 30^\circ$ for SA-Ca+Na layers to $<5^\circ$ for
42
43 SA-Na layers. This very strong dependence of the contact angle on the counter ion species is
44
45 the key observation of the present study. Since the contact angles of water on stable self-
46
47 assembled monolayers such as alkylsilane layers on glass and alkylthiol layers on Au with a
48
49 comparable length of the alkyl chain are known to be close to 110° ³⁴, these results clearly
50
51 show that the LB films of SA in our experiments do not remain intact upon exposure to water
52
53 but decompose at least partially. The large variation of θ_e for the three different subphases
54
55 suggests that the degree of decomposition varies substantially depending on the specific
56
57
58
59
60

cation present in the subphase: SA-Ca layers seem to remain largely intact, SA-Na layers seem to be largely removed, and SA-Ca+Na layers show an intermediate behavior.

Qualitatively similar results were obtained for a large number of samples, also including mica substrates instead of oxidized silicon wafers. The trends regarding the stabilizing effect of Ca^{2+} in the subphase on θ_e were consistently found (see Fig 2a). Yet, the absolute values of θ_e vary substantially depending on details of the sample cleaning, preparation, and drying protocol. Occasionally, θ_e could be as low as 30° even for SA-Ca monolayers (supporting information).

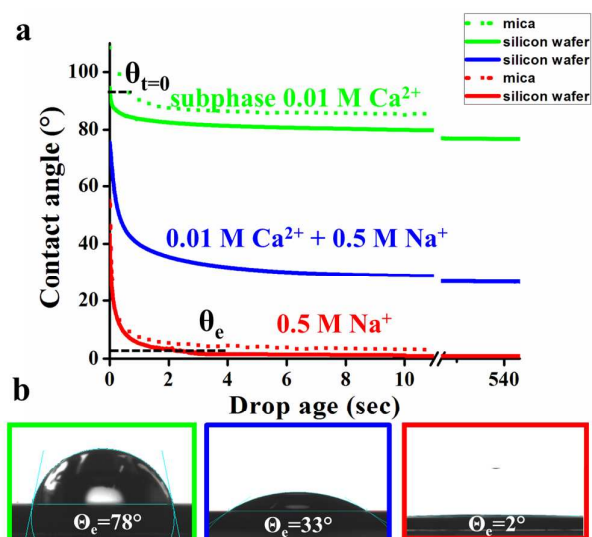


Figure 2. (color online) Macroscopic wettability of three monolayers: SA-Ca (green), SA-Ca+Na (blue), and SA-Na (red). (a) Time evolution of the contact angle and (b) snapshots of drops in the final state showing the equilibrium contact angles (θ_e). Note: the axis break in (a) showing the final equilibrium angle.

These wettability changes could originate from different processes at the microscopic level. For example they could be due to desorption of the SA molecules upon exposure of the layer to the aqueous drop. But alternatively they might also result from structural rearrange-

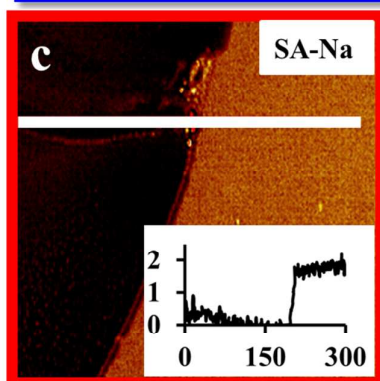
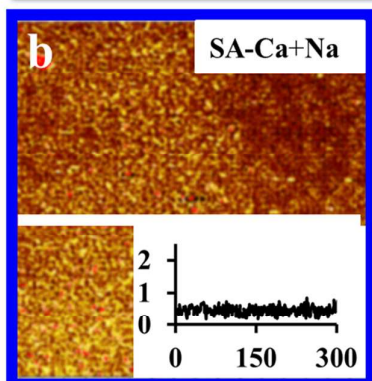
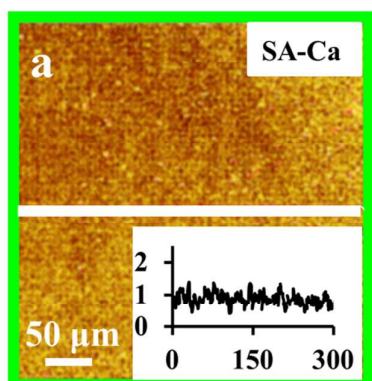
1
2
3 ments within the layer, such that hydrophilic headgroups become exposed to the aqueous
4 liquid. To distinguish between the different possible scenarios, we performed additional
5 characterizations aimed at the surface morphology. Images of the layers (after removing the
6 drop and drying the samples) obtained with ellipsometry and AFM are shown in Fig. 3.
7
8
9

10
11
12 For the SA-Ca and SA-Ca+Na samples, both ellipsometry and AFM images recorded
13 in the central area of the original drop look similar, as can be seen in Fig. 3a, b) and 3a', b').
14 Ellipsometry indicates a more or less homogeneous coverage with an average thickness of
15 about 1 nm in the former case and approximately 0.5 nm for the latter samples. Both values
16 are substantially lower than the 2 nm corresponding to the all-*trans* length of SA molecules
17 before they were exposed to the water drop. Hence we conclude that the LB monolayers must
18 have been partially desorbed.
19
20
21
22
23
24
25
26
27
28

29 For SA-Na samples (Fig. 3c and c'), the situation is clearly different and the residual
30 thickness after water exposure is essentially zero. When we image the edge of the region
31 exposed to the water drop, a clear contrast is seen between the exposed area with now bare
32 substrate and the intact monolayer around it. Also the shape of the edge of the drop is
33 observed for larger scan size (20-30 μm) AFM images (not shown) as seen with ellipsometry
34 in Fig. 3c. While the poor lateral resolution of imaging ellipsometry precludes a more detailed
35 analysis, AFM imaging reveals the details of the decomposition process: the monolayers
36 partially desorb from the substrate, leaving behind areas covered by the original SA film
37 (bright in Fig. 3a' and b') and holes (dark) exposing what seems to be the bare substrate. The
38 phase image (Fig. 4a) also reveals a clear contrast between the high and the low level, which
39 discriminate between different types of materials, supporting the interpretation that the lower
40 level is indeed the bare substrate. From histograms of the height distribution (right part of Fig.
41 3 a', b', and c') we extract the area fraction and the thickness of the residual film. The latter is
42
43
44
45
46
47
48
49
50
51
52
53
54
55
56
57
58
59
60

1
2
3 approximately 2 nm, in agreement with the all-*trans* length of the SA molecules. Since the
4
5 missing SA molecules are not found at the surface and they are insoluble in water at pH=6,
6
7 we think that they migrated to the air-water interface and were washed away upon removal of
8
9
10 the drop.
11
12
13
14
15

Ellipsometry



AFM

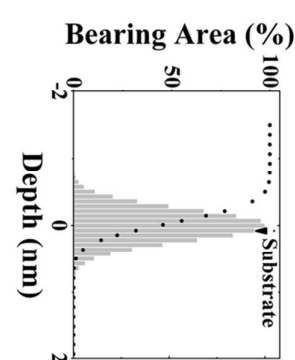
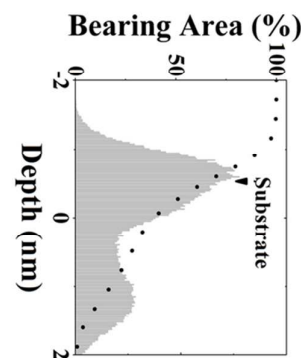
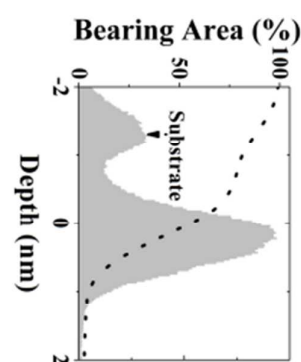
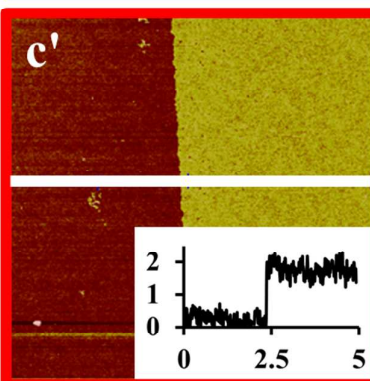
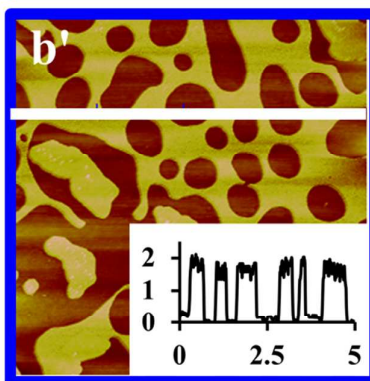
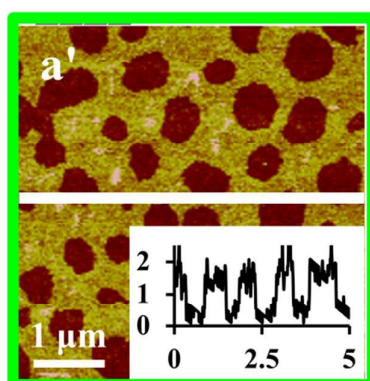


Figure 3. (color online) Macroscopic and microscopic images of SA-Ca (a and a'), SA-Ca+Na (b and b') and SA-Na monolayer (c and c') after exposure to water. a, b and c: imaging ellipsometry; a', b' and c': AFM). Inset images are height profiles corresponding to the white scan line (abscissa in μm ; ordinate in nm). Histograms in a', b', and c' show the frequency and cumulative bearing area of the height levels.

For the SA-Na samples, AFM images confirm the results of the ellipsometry measurements. Within the previous contact area of the drop, the samples are perfectly flat. As we image the edge of the contact area, a clear topographic step is found with a height of ~ 1.5 nm, as in the case of the holes in the layers on the SA-Ca and SA-Ca+Na samples. Again, the topographic step is accompanied by a jump in the phase images, confirming the idea of different material compositions.

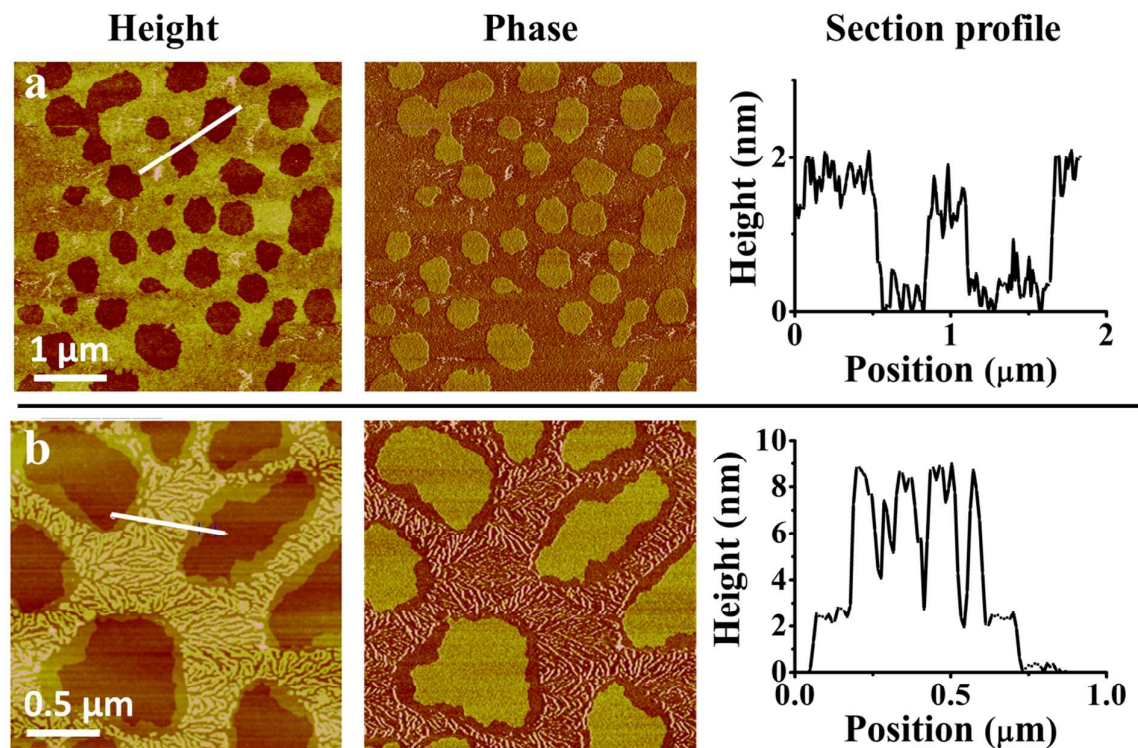


Figure 4. AFM height and phase images along with section profiles for (a) SA-Ca monolayer

1
2
3 *exposed to water and (b) SA-Ca+Na monolayer exposed to 0.01 M CaCl₂ solution. The*
4 *different contrasts correspond to bare substrate, monolayer and multilayer.*
5
6
7

8 These observations unequivocally demonstrate that our LB layers of SA partially
9 decompose upon exposure to water. The somewhat reduced height (as compared to the all-
10 *trans* length of the SA molecules) of the steps in the AFM images suggests that the molecules
11 in the residual layer are either slightly tilted or that the 'bare' substrate in the holes is in fact
12 still covered by a sub-monolayer of hydrocarbon chains oriented parallel to the substrate. The
13 present data do not allow drawing a definite conclusion in this respect. Notwithstanding this
14 uncertainty, all data clearly and consistently demonstrate that Ca²⁺ ions in the subphase have
15 strong stabilizing effect on the SA layers, whereas Na⁺ ions do not.
16
17
18
19
20
21
22
23
24
25
26

27 **2. Effects of salinity of exposure water on monolayer stability:**

28
29

30 Having demonstrated the stabilizing effect of Ca²⁺ ions in the subphase during
31 preparation of the LB layers, we now address the effects of ions in the exposure solution. We
32 focus again on Na⁺ and Ca²⁺ ions. In addition to the pure water discussed in the previous
33 section, 0.01 M and 0.1 M NaCl, as well as CaCl₂ are used as the exposure solutions.
34
35
36
37
38
39

40 Figure 5a shows the time evolution of the contact angle for the five different exposure
41 solutions on SA-Ca monolayers. The data for pure water are the same as in Fig. 2a. The other
42 exposure solutions display the same qualitative behavior, yet it is clear that θ_e is larger for
43 higher salt concentrations. The highest value of $\theta_e \sim 95^\circ$ is obtained for the 0.1 M CaCl₂
44 solution. The contact angle after 10 min (not shown) is only slightly smaller than after 30 s,
45 like in Fig. 2. Similar results are found for samples prepared with the two other subphase
46 compositions. As summarized in Fig. 5b, more ions in the exposure solution lead to larger
47 contact angles on the SA layers in all cases. Again, Ca²⁺ ions are - by and large - more
48
49
50
51
52
53
54
55
56
57
58
59
60

efficient than Na^+ ions at stabilizing the LB films. Note, however, that the overall effect of ions in the exposure solution is only of order 10° and thus much less pronounced than for ions in the subphase.

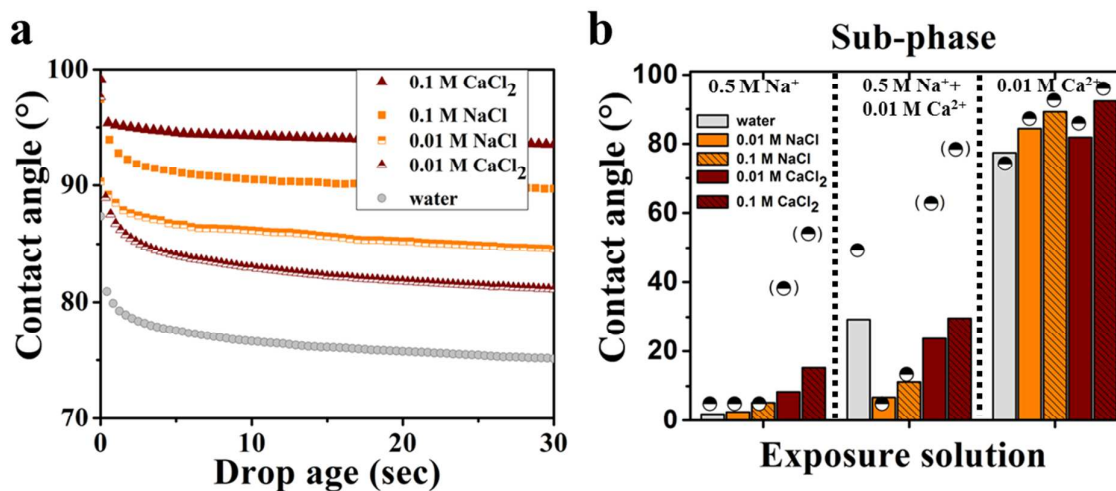


Figure 5. (a) Contact angle vs. time on SA-Ca monolayer for various compositions of exposure solution. (b) Equilibrium contact angles for all compositions of subphase and exposure solution (bars: experimental results from contact angle goniometry; symbols: values extracted from AFM images in combination with Cassie equation (see text for details)).

In Fig. 6 we show an overview of AFM micrographs obtained for all combinations of the composition of subphase and exposure solution investigated in this study. Desorbed area fractions are calculated from histograms of the height distribution as in Fig. 3. Comparing the different subphases, it is clear that LB films prepared on the subphase containing CaCl_2 are the most stable. We find that for an exposure solution of 0.1 M CaCl_2 , as little as $A_{des} = 6\%$ of the SA-Ca film decomposes. This percentage increases for exposure solutions containing less Ca^{2+} or containing Na^+ . The depth of the holes remains close to 2 nm, with only very small area fractions of thicker films in the case of NaCl exposure solutions. The maximum desorbed

1
2
3 area amounts to 38%, indicating a fairly good stability of the LB film upon contact with
4
5 water. The value of 38% is reproducible within $\pm 3\%$ for at least 5 consecutive experiments.
6
7

8 For subphases containing 0.5 M NaCl (with or without additionally 0.01 M CaCl₂), a
9
10 dramatically different picture is found. For exposure solutions containing NaCl, the LB films
11
12 are decomposed more or less completely, indicated by desorption ratios A_{des} close to 100%.
13
14 For exposure solutions containing CaCl₂ we also find large areas of bare substrate but still a
15
16 finite amount covered by a layer. Interestingly, in this case the thickness of the residual layers
17
18 largely exceeds the initial 2 nm. We attribute this to the formation of double or multilayers.
19
20 Substrates with bare areas, monolayers and multilayers were already shown in Fig. 4b for one
21
22 of these samples. The chemical nature and in particular the termination of the multilayers are
23
24 not clear. Yet, we suspect that the multilayers contain calcium stearate and that they expose
25
26 the hydrophilic head groups to the aqueous phase (see discussion below). This compound is
27
28 known to be a particularly stable, which was – amongst others – found to precipitate easily at
29
30 oil-water interfaces if dissolved in oil.⁸ (Few images also display very high round features that
31
32 look very different from the decomposed areas of the film. We identify these features as salt
33
34 crystallites that appear as we blow off the residual drop and dry the sample).
35
36
37
38
39

40 To examine the consistency between our macroscopic contact angle measurements and
41
42 the microscopic characterizations using AFM, we calculate theoretical contact angles, by
43
44 combining the area fraction obtained from the AFM images with Cassie's equation for the
45
46 contact angle of heterogeneous surfaces $\cos \theta = f_1 \cos \theta_1 + f_2 \cos \theta_2$ (f_i , θ_i : area fraction and
47
48 contact angle of phase i ; i =LB film, substrate.) Using a Young angle of $\theta_1=100^\circ$ for the LB
49
50 film and $\theta_2=5^\circ$ for the bare substrate and taking $f_1=1-A_{des}$ and $f_2=A_{des}$ from Fig. 6, we find the
51
52 contact angles indicated by the round symbols shown in Fig. 5b. (Here, the values of θ_1 and θ_2
53
54 are typical values for the contact angle of compact layers of self-assembled monolayers and
55
56
57
58
59
60

1
2
3 cleaned silica surfaces, respectively.³⁵⁻³⁶ Note that the absolute values are not very critical and
4
5 may be varied by 5° without substantial impact on the agreement with the experimental data.)
6
7 Despite the rather wide range of A_{des} covered for the various conditions, the values for θ
8
9 calculated from the AFM images agree within 10% with the macroscopic measurements. Note
10
11 that the success of the Cassie equation is not trivial. It implies in the first place that the
12
13 variations observed in the center of the solid-liquid interfacial area are representative of the
14
15 local (de)composition at the contact line, *i.e.* at the location where the contact angle is
16
17 determined. (This aspect has been discussed intensively in recent years following up a critical
18
19 note by Gao and McCarthy).³⁷⁻³⁹ Second, the agreement suggests that the advancing contact
20
21 angle that we measure under the conditions of our slowly spreading drops is indeed close to
22
23 the equilibrium angle, as determined by Cassie's equation. This is again not trivial since the
24
25 closeness of the Cassie angle to the advancing and receding angle depends on the nature of
26
27 the defects with respect to the majority species on the surface as pointed out by Priest et al.⁴⁰
28
29
30
31

32
33 The SA-Ca+Na and SA-Na films exposed to CaCl₂ solutions (symbols in parenthesis)
34
35 deviate from this general trend. These, however, are the samples shown in the bottom right
36
37 quadrant of Fig. 6, which display the formation of multilayers after exposure to the electrolyte
38
39 solution. Their experimental contact angle is much smaller than the one predicted by Cassie's
40
41 law under the assumption $\theta_1=100^\circ$. This apparent discrepancy disappears however, if we
42
43 assume that the multilayers are not terminated by the hydrophobic tail but rather expose the
44
45 hydrophilic carboxylic acid group towards the solution, leading to a much smaller value of θ_1
46
47 (see phase contrast corresponding to multilayer formation in Fig. 4b). This behavior is
48
49 consistent with observations in other experiments with decomposing surfactant layers.¹³
50
51
52
53
54
55
56
57
58
59
60

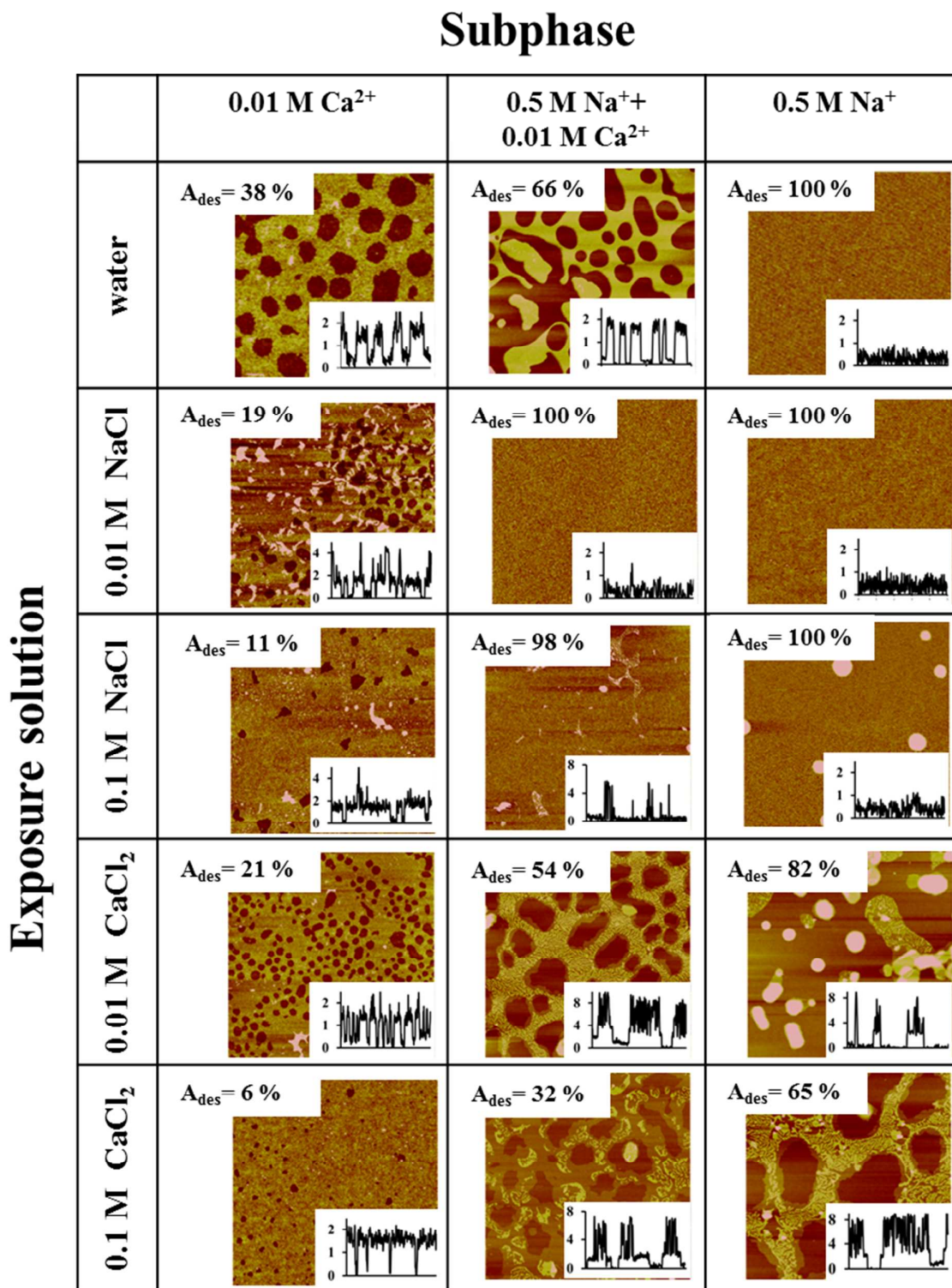


Figure 6. AFM viewgraphs of LB films prepared with all combinations of subphases after exposure to water and liquid compositions. Image size: $5 \times 5 \mu\text{m}^2$. Desorption area A_{des} indicates area fraction of exposed bare substrate. Insets show representative cross sections. Vertical scale: in nm. Horizontal scale: $5 \mu\text{m}$.

1
2
3 The behavior of the SA-Ca+Na films in pure water cannot be explained in this manner.
4
5 The thickness of the residual film is close to 2 nm, as concluded from the depth of the holes in
6
7 film. The desorption ratio suggests that approximately one third of the layer should still be
8
9 present in its original form with a hydrophobic termination exposed to the water. It leads to a
10
11 contact angle of approximately 50° by calculating with Cassie's equation, exceeding the
12
13 experimental value by ~20°. We do not have any explanation for this deviation, which has
14
15 been found to persist over several independent measurements spread over a period of several
16
17 months.
18
19

20 21 **DISCUSSION**

22
23
24 Overall, our experiments clearly show that the presence of Ca²⁺ ions (whether from
25
26 the subphase or from the exposure solution) strongly stabilizes LB films of stearic acid
27
28 deposited on silica surfaces.^{24, 41-46} To discuss the stabilization mechanism, we consider the
29
30 preparation of the LB film and its subsequent decomposition upon exposure to aqueous liquid
31
32 separately. Fig. 7 sketches the relevant processes during adsorption-desorption of the
33
34 monolayer. The Langmuir film initially residing on the subphase consists of a close-packed
35
36 layer of stearate molecules (Fig. 7a). The structure and stability of this Langmuir monolayer
37
38 are known to change in different ways, depending on the presence of mono- and divalent ions,
39
40 as well as the pH in the subphase. At sufficiently high pH, monovalent cations in the subphase
41
42 cause the monolayer to become less ordered. Divalent cations (at sufficiently high pH) have
43
44 the opposite effect: they effectively compress the monolayer into a tightly packed untilted
45
46 structure, leading to enhanced crystalline order⁴⁷, changes in viscoelastic response⁴⁸, and
47
48 make it more easily transferable to solid substrates.²⁹
49
50
51
52
53
54
55
56
57
58
59
60

1
2
3 In this work, the subphase pH is chosen high enough to ensure that the carboxylic acid
4 groups are largely deprotonated. The ionization fraction of the molecules at the interface (χ)
5 has been related to the pH of the subphase by the Gouy-Chapman equation^{24, 49}
6
7
8
9

$$10 \quad \text{pH}_{\text{subphase}} = \text{pK}_a + \log\left(\frac{\chi}{1-\chi}\right) + \frac{0.87}{z} \sinh^{-1}\left(\frac{136\chi}{A\sqrt{c}}\right),$$

11
12
13 where z is the valency of the ions, A is the molecular area (\AA^2) and c is the concentration of
14 the counterions (moles/L). Inserting $\text{pK}_a = 5.6$ ⁵⁰ and using the aqueous compositions in our
15 experiments, we obtain a deprotonation ratio of 86.4% for 0.01 M CaCl_2 and 82.3% for 0.5
16 M NaCl solutions at pH 9.5. According to literature, divalent cations (D^{2+}) can form different
17 complexes with ionized stearic acid ($\text{R}^- = \text{CH}_3(\text{CH}_2)_{16} \text{COO}^-$): positive RD^+ , neutral R_2D or
18 both of these complexes simultaneously.⁵¹⁻⁵⁴ The presence of both R^- and RD^+ can make the
19 Langmuir layer electrically neutral at high pH, as has been found for Ca^{2+} both theoretically^{51,}
20
21
22
23
24
25
26
27
28
29
30
31
32
33
34
35
36
37
38
39
40
41
42
43
44
45
46
47
48
49
50
51
52
53
54
55
56
57
58
59
60
and therefore the monolayer remains mainly negatively charged because of dissociated R^- .⁵¹

When we transfer these neutral or negatively charged layers to our silica substrates,
they come in contact with a negatively charged surface^{43-44,57} (Fig. 7b). Under these
conditions, positively charged SACa^+ (RD^+) moieties can associate with negatively charged
sites on the silica surface to form strongly bound neutral complexes. Neutral SA_2Ca (R_2D) can
be stabilized by lateral interactions (van der Waals and hydrophobic forces) between alkyl
chains which can also lead to a strongly bound LB film.⁵⁸ In the contrasting case of sublayers
containing only Na^+ cations, a partially dissociated Langmuir layer, carrying some negative
charges, is deposited onto a strongly negatively charged solid surface. This precludes the
collective self-assembly of cation-stabilized complexes between stearate molecules and
deprotonated silanol (SiO^-) groups. Moreover, charge neutrality will require the incorporation

of even more cations between the film and the substrates to compensate for the excess negative charges. The combination of both aspects leads to an LB film which can only be weakly bound to the substrate and stabilized by only lateral interactions within the film presumably.

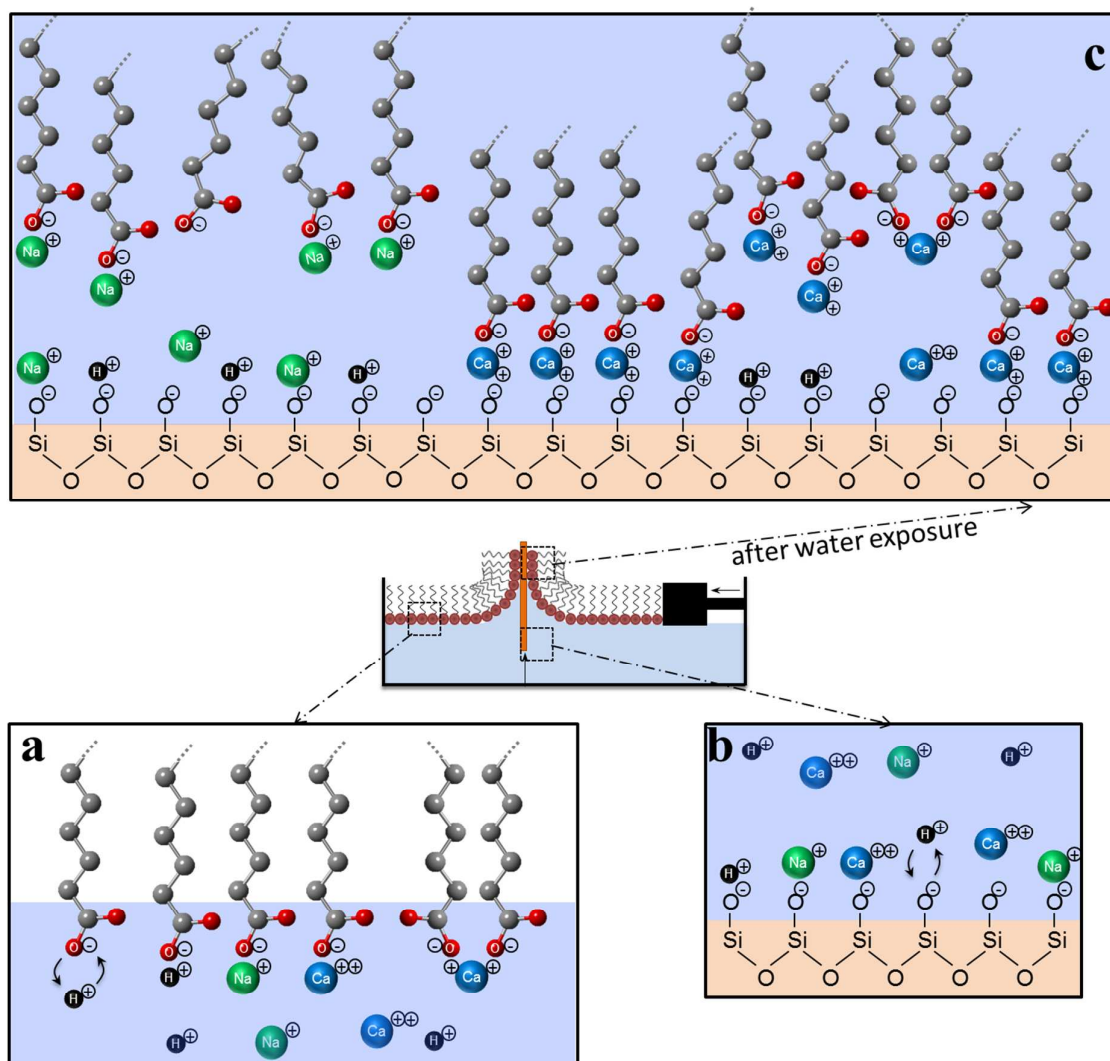


Figure 7. Schematic illustration of monolayer adsorption-desorption process (a) formation of salt complexes with dissociated fatty acid at air–water interface (b) negatively charged substrate dipped under subphase (c) desorption of monolayer after water exposure.

1
2
3 The behavior of the SA-Ca+Na films with the mixed subphases is more complex. The
4 partial stability of the layers upon exposure to pure water suggests that some adsorbed Ca^{2+} is
5 present and able to stabilize the LB films. However, this stabilization is clearly not as strong
6 as in the case of a pure 0.01 M CaCl_2 subphase. The competition between the stronger binding
7 Ca^{2+} ions and the 50 times more concentrated Na^+ ions in the subphase leads to a mixed
8 association of R^- and SiO^- with the two cationic species. Upon exposure to pure NaCl
9 solutions, the gradients in chemical potential for Ca^{2+} and Na^+ apparently lead to a complete
10 destabilization of the films, suggesting that Ca^{2+} and/or SACa^+ ions initially stabilizing the
11 LB film can be exchanged with Na^+ ions from the bulk exposure solution resulting in the
12 complete decomposition of layer. The behavior upon exposure to pure Ca^{2+} solutions again
13 suggests an exchange of ions between the bulk solution and loosely bound parts of the LB
14 monolayer.
15
16
17
18
19
20
21
22
23
24
25
26
27
28
29

30 Such rearrangements are not uncommon. For multilayer LB films, they have been studied in
31 great detail.^{10,12,29} In particular, X-ray reflectivity and X-ray photoemission spectroscopy
32 demonstrated a very strong mobility and exchange of cations bound in LB multilayers.⁹ These
33 studies also suggest that ion exchange is facilitated by swelling of the LB films. To explore
34 this possibility, we performed some additional ‘*in-situ*’ AFM experiments, in which the LB
35 films were imaged under aqueous liquid (instead of air). These experiments showed film
36 decomposition patterns that are consistent with the *ex-situ* experiments (see Supporting
37 Information). However, the depth of the holes in the LB films is more than twice as large as in
38 the *ex-situ* images recorded on the same surface after drying. Explanations for this swelling
39 behavior and other possible rearrangements (e.g. tilting as a result of partial desorption) are
40 the subject of an ongoing follow-up study.
41
42
43
44
45
46
47
48
49
50
51
52
53
54
55
56
57
58
59
60

1
2
3 The Ca^{2+} -induced stabilization of LB films might also provide a strategy to develop more
4
5 stable hydrophobic layers for surface forces measurements. Investigations of fundamental
6
7 interaction forces between hydrophobic surfaces immersed into water have long been
8
9 compromised by problems with the stability of hydrophobic layers.^{13,16} LB films stabilized by
10
11 Ca^{2+} or even higher valence cations might provide a route to overcome these problems.
12

13
14
15 Overall, the observations described in this work are consistent with the multiple ion exchange
16
17 mechanism of the low salinity water flooding process as proposed by Lager et al.⁵ Ionically
18
19 bound layers of SA on silica surfaces indeed partially come off the solid surface and render it
20
21 more hydrophilic if exposed to pure water rather than highly saline electrolytes. As in core
22
23 flooding oil recovery experiments divalent ions also play a crucial role in the present generic
24
25 model system. It is interesting to note, though, that ions present in the subphase during the
26
27 preparation of the LB films have a stronger influence than those added subsequently to the
28
29 exposure solution. This might suggest that the salinity of the formation water, which was
30
31 present when the oil invaded a certain initially water saturated reservoir rock, plays an
32
33 important role for the stability of the hydrophobizing layers and thus for the subsequent
34
35 success of low salinity water flooding. While it is encouraging that the same qualitative
36
37 behavior is also found on mica substrates (serving as a model for clays that are typically
38
39 present in many rock formations), more extensive experiments involving different classes of
40
41 polar organic components from crude oil obviously need to be performed to confirm the
42
43 general applicability of the multivalent ion exchange concept.
44
45
46
47
48

49 **CONCLUSIONS**

50
51
52 The stability of Langmuir Blodgett films of stearic acid upon exposure to water is strongly
53
54 enhanced by the presence of Ca^{2+} ions. Strongly bound LB films transferred in the presence of
55
56 an excess of Ca^{2+} are very stable independent of the composition of the aqueous phase it is
57
58
59
60

1
2
3 exposed to, suggesting that Ca^{2+} can efficiently bind negatively charged SA to negatively
4 charged surfaces. In contrast, Na^+ ions are unable to provide such stabilization. For weakly
5 bound LB films transferred in the presence of mixtures of Na^+ and Ca^{2+} , high concentrations
6 of Na^+ in the ambient exposure fluid can even destabilize ionically bound organic layers. This
7 destabilization can be rationalized by the replacement of initially present stabilizing Ca^{2+} ions
8 implying a rapid exchange of ions between the ionic layer binding the LB film to the substrate
9 and the ambient electrolyte. Clearly, the competition of several simultaneously present ionic
10 species, which is characteristic for most geological, biological, and technological
11 environments, adds substantial complexity and deserves additional attention in future research.
12
13

14
15 From an applied perspective, the Ca^{2+} -induced stabilization reported here implies a
16 destabilization and easy removal of ionically bound organic layers in the absence of divalent
17 ions. This is desired in the context of enhanced oil recovery. We anticipate that the fatty acid
18 layers investigated can indeed be exploited as a model system for further studies of various
19 complex geophysical and technological processes in well-defined laboratory experiments.
20
21
22

23
24
25
26
27
28
29
30
31
32
33
34
35
36 **Acknowledgements:** We thank Daniel Wijnperle and Mariska van der Weide for technical
37 support, and Dirk van den Ende for critical reading of this manuscript. We acknowledge
38 financial support within the ExploRe research program of BP plc.
39
40
41

42
43
44 **Supporting Information Available:** Effects of preparation conditions on the water contact
45 angle and the morphology (in air and under water) of Langmuir-Blodgett layers of Stearic
46 Acid on silica substrates. This material is available free of charge via the Internet at
47 <http://pubs.acs.org>.
48
49
50
51
52
53
54
55
56
57
58
59
60

REFERENCES

1. Tredgold, R. H.; Vickers, A. J.; Allen, R. A., Structural Effects on the Electrical-Conductivity of Langmuir-Blodgett Multilayers of Cadmium Stearate. *J. Phys. D* **1984**, *17* (1), L5-L8.
2. Swalen, J. D.; Allara, D. L.; Andrade, J. D.; Chandross, E. A.; Garoff, S.; Israelachvili, J.; McCarthy, T. J.; Murray, R.; Pease, R. F.; Rabolt, J. F.; Wynne, K. J.; Yu, H., Molecular Monolayers and Films. *Langmuir* **1987**, *3* (6), 932-950.
3. Briscoe, W. H.; Titmuss, S.; Tiberg, F.; Thomas, R. K.; McGillivray, D. J.; Klein, J., Boundary lubrication under water. *Nature* **2006**, *444* (7116), 191-194.
4. Ohmori, S.; Ito, S.; Yamamoto, M., Layered Structure of Langmuir-Blodgett Polymer-Films Measured by Interlayer Energy-Transfer. *Macromolecules* **1991**, *24* (9), 2377-2384.
5. Lager, A., Webb, K. J., Black, C. J. J., Singleton, M, Sorbie, K. S, Low Salinity Oil Recovery - An Experimental Investigation. In *International Symposium of the Society of Core Analysts*, SCA2006-36: Trondheim, Norway, 2006.
6. Simoni, S. F.; Bosma, T. N. P.; Harms, H.; Zehnder, A. J. B., Bivalent cations increase both the subpopulation of adhering bacteria and their adhesion efficiency in sand columns. *Environ. Sci. Technol.* **2000**, *34* (6), 1011-1017.
7. Pastre, D.; Pietrement, O.; Fusil, P.; Landousy, F.; Jeusset, J.; David, M. O.; Hamon, C.; Le Cam, E.; Zozime, A., Adsorption of DNA to mica mediated by divalent counterions: A theoretical and experimental study. *Biophys. J.* **2003**, *85* (4), 2507-2518.
8. de Rooter, R.; Tjerkstra, R. W.; Duits, M. H. G.; Mugele, F., Influence of Cationic Composition and pH on the Formation of Metal Stearates at Oil–Water Interfaces. *Langmuir* **2011**, *27* (14), 8738-8747.

- 1
2
3 9. Ganguly, P.; Pal, S.; Sastry, M.; Shashikala, M. N., Spontaneous Self-Organization
4
5 Via Cation-Exchange in Fatty-Acid Films Immersed in Aqueous-Media. *Langmuir* **1995**, *11*
6
7 (4), 1078-1080.
8
- 9
10 10. Schwartz, D. K.; Viswanathan, R.; Zasadzinski, J. A. N., Reorganization and
11
12 Crystallite Formation in Langmuir-Blodgett-Films. *J. Phys. Chem.* **1992**, *96* (25), 10444-
13
14 10447.
15
- 16
17 11. Gosvami, N. N.; Parsons, E.; Marcovich, C.; Berkowitz, M. L.; Hoogenboom, B. W.;
18
19 Perkin, S., Resolving the structure of a model hydrophobic surface: DODAB monolayers on
20
21 mica. *RSC Adv.* **2012**, *2* (10), 4181-4188.
22
- 23
24 12. Ye, S.; Noda, H.; Nishida, T.; Morita, S.; Osawa, M., Cd²⁺-induced interfacial
25
26 structural changes of Langmuir-Blodgett films of stearic acid on solid substrates: A sum
27
28 frequency generation study. *Langmuir* **2004**, *20* (2), 357-365.
29
- 30
31 13. Perkin, S.; Kampf, N.; Klein, J., Stability of self-assembled hydrophobic surfactant
32
33 layers in water. *J. Phys. Chem. B* **2005**, *109* (9), 3832-3837.
34
- 35
36 14. Chevalier, N. R.; Chevillard, C.; Guenoun, P., Monovalent Cations Trigger Inverted
37
38 Bilayer Formation of Surfactant Films. *Langmuir* **2010**, *26* (20), 15824-15829.
39
- 40
41 15. Christenson, H. K.; Claesson, P. M., Direct measurements of the force between
42
43 hydrophobic surfaces in water. *Adv. Colloid Interface Sci.* **2001**, *91* (3), 391-436.
44
- 45
46 16. Meyer, E. E.; Rosenberg, K. J.; Israelachvili, J., Recent progress in understanding
47
48 hydrophobic interactions. *Proc. Natl. Acad. Sci. U. S. A.* **2006**, *103* (43), 15739-15746.
49
- 50
51 17. Secombe, J. L., A.; Jerauld, G.; Jhaveri, B.; Buikema, T.; Bassler, S.; Denis, J.;
52
53 Webb, K. J.; Cockin, A.; Fueg, E. , Demonstration of Low-Salinity EOR at Interwell Scale,
54
55 Endicott Field, Alaska. In *SPE Improved Oil Recovery Symposium*, Tulsa, OK, 2010.
56
- 57
58 18. Yazdanian, M.; Yu, H.; Zograf, G.; Kim, M. W., Divalent cation-stearic acid
59
60 monolayer interactions at the air/water interface. *Langmuir* **1992**, *8* (2), 630-636.

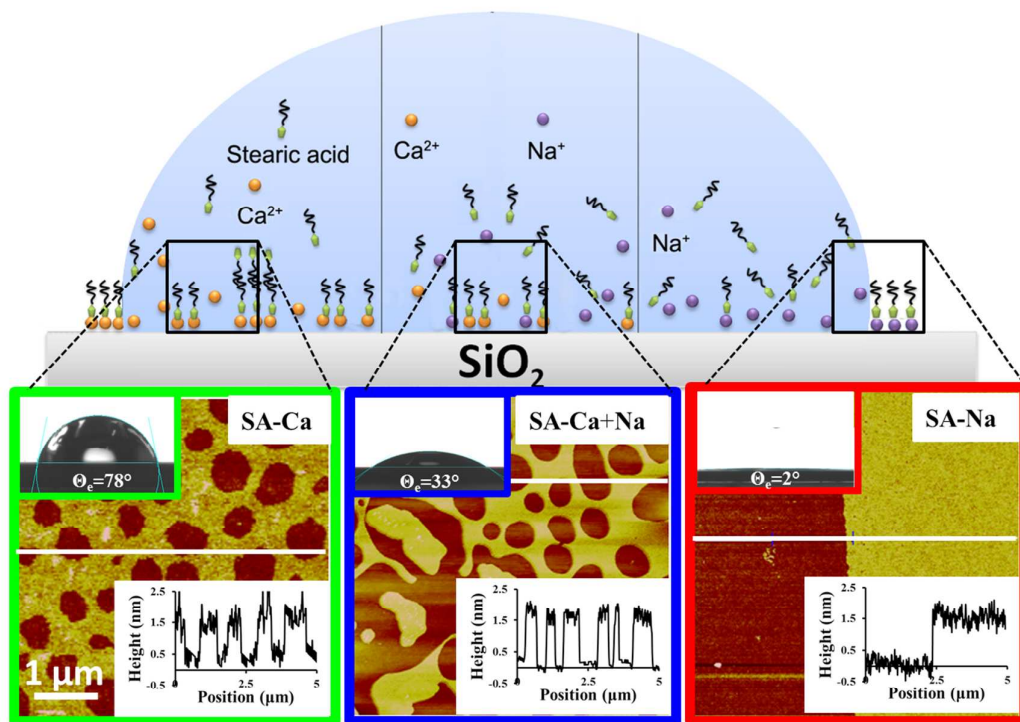
- 1
2
3 19. Bloch, J. M.; Yun, W. B.; Yang, X.; Ramanathan, M.; Montano, P. A.; Capasso, C.,
4
5 Adsorption of Counterions to a Stearate Monolayer Spread at the Water-Air Interface: A
6
7 Synchrotron X-Ray Study. *Phys. Rev. Lett.* **1988**, *61* (26), 2941-2944.
8
9
10 20. Gericke, A.; Huehnerfuss, H., In situ investigation of saturated long-chain fatty acids
11
12 at the air/water interface by external infrared reflection-absorption spectrometry. *J. Phys.*
13
14 *Chem.* **1993**, *97* (49), 12899-12908.
15
16 21. Ye, S.; Noda, H.; Morita, S.; Uosaki, K.; Osawa, M., Surface molecular structures of
17
18 Langmuir-Blodgett films of stearic acid on solid substrates studied by sum frequency
19
20 generation spectroscopy. *Langmuir* **2003**, *19* (6), 2238-2242.
21
22
23 22. Blodgett, K. B., Films built by depositing successive monomolecular layers on a solid
24
25 surface. *J. Am. Chem. Soc.* **1935**, *57* (6), 1007-1022.
26
27
28 23. Langmuir, I., Overturning and anchoring of monolayers. *Science* **1938**, *87*, 493-500.
29
30 24. Kundu, S.; Langevin, D., Fatty acid monolayer dissociation and collapse: Effect of pH
31
32 and cations. *Colloids Surf., A* **2008**, *325* (1-2), 81-85.
33
34 25. Aveyard, R.; Binks, B. P.; Carr, N.; Cross, A. W., Stability of Insoluble Monolayers
35
36 and Ionization of Langmuir-Blodgett Multilayers of Octadecanoic Acid. *Thin Solid Films*
37
38 **1990**, *188* (2), 361-373.
39
40 26. Goddard, E., Ionizing monolayers and pH effects. *Adv. Colloid Interface Sci.* **1974**, *4*
41
42 (1), 45-78.
43
44 27. Gershevit, O.; Sukenik, C. N., In situ FTIR-ATR analysis and titration of carboxylic
45
46 acid-terminated SAMs. *J. Am. Chem. Soc.* **2004**, *126* (2), 482-3.
47
48 28. Brzozowska, A. M.; Duits, M. H. G.; Mugele, F., Stability of stearic acid monolayers
49
50 on Artificial Sea Water. *Colloids Surf., A* **2012**, *407* (0), 38-48.
51
52
53 29. Zasadzinski, J. A.; Viswanathan, R.; Madsen, L.; Garnæs, J.; Schwartz, D. K.,
54
55 Langmuir-Blodgett-Films. *Science* **1994**, *263* (5154), 1726-1733.
56
57
58
59
60

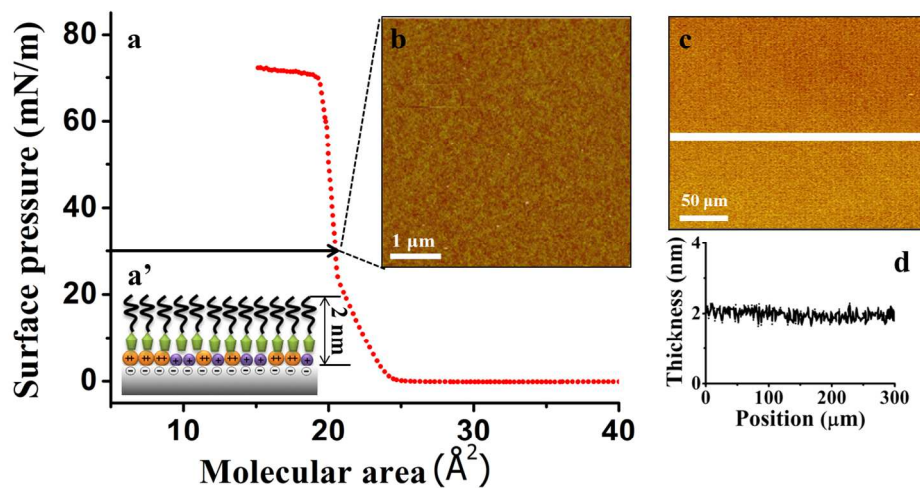
- 1
2
3 30. Graber, E. R.; Tagger, S.; Wallach, R., Role of Divalent Fatty Acid Salts in Soil Water
4
5 Repellency. *Soil Sci. Soc. Am. J.* **2009**, *73* (2), 541-549.
6
7
8 31. Tompkins, H. G. I., E.A, *Handb. Ellipsom.* Springer: 2005.
9
10 32. Shaitan, K.; Pustoshilov, P., Molecular Dynamics of a Stearic Acid Monolayer.
11
12 *Biophysics* **1999**, *44* (3), 429-434.
13
14 33. Bird, J. C.; Mandre, S.; Stone, H. A., Short-Time Dynamics of Partial Wetting. *Phys.*
15
16 *Rev. Lett.* **2008**, *100* (23), 234501-4.
17
18 34. Love, J. C.; Estroff, L. A.; Kriebel, J. K.; Nuzzo, R. G.; Whitesides, G. M., Self-
19
20 assembled monolayers of thiolates on metals as a form of nanotechnology. *Chem. Rev.* **2005**,
21
22 *105* (4), 1103-1170.
23
24 35. Ren, S. L.; Yang, S. R.; Wang, J. Q.; Liu, W. M.; Zhao, Y. P., Preparation and
25
26 tribological studies of stearic acid self-assembled monolayers on polymer-coated silicon
27
28 surface. *Chem. Mater.* **2004**, *16* (3), 428-434.
29
30 36. Tao, Y. T., Structural comparison of self-assembled monolayers of n-alkanoic acids on
31
32 the surfaces of silver, copper, and aluminum. *J. Am. Chem. Soc.* **1993**, *115* (10), 4350-4358.
33
34 37. Gao, L.; McCarthy, T. J., How Wenzel and Cassie Were Wrong. *Langmuir* **2007**, *23*
35
36 (7), 3762-3765.
37
38 38. Panchagnula, M. V.; Vedantam, S., Comment on How Wenzel and Cassie Were
39
40 Wrong by Gao and McCarthy. *Langmuir* **2007**, *23* (26), 13242; discussion 13243.
41
42 39. McHale, G., Surface free energy and microarray deposition technology. *Analyst* **2007**,
43
44 *132* (3), 192-5.
45
46 40. Priest, C.; Sedev, R.; Ralston, J., Asymmetric Wetting Hysteresis on Chemical
47
48 Defects. *Phys. Rev. Lett.* **2007**, *99* (2), 026103-4.
49
50
51
52
53
54
55
56
57
58
59
60

- 1
2
3 41. Tang, C. Y.; Allen, H. C., Ionic Binding of Na⁺ versus K⁺ to the Carboxylic Acid
4 Headgroup of Palmitic Acid Monolayers Studied by Vibrational Sum Frequency Generation
5 Spectroscopy†. *J. Phys. Chem. A* **2009**, *113* (26), 7383-7393.
6
7
8
9
10 42. Tang, C. Y.; Huang, Z.; Allen, H. C., Interfacial Water Structure and Effects of Mg²⁺
11 and Ca²⁺ Binding to the COOH Headgroup of a Palmitic Acid Monolayer Studied by Sum
12 Frequency Spectroscopy. *J. Phys. Chem. B* **2010**, *115* (1), 34-40.
13
14
15
16 43. Besteman, K.; Zevenbergen, M. A. G.; Heering, H. A.; Lemay, S. G., Direct
17 observation of charge inversion by multivalent ions as a universal electrostatic phenomenon.
18 *Phys. Rev. Lett.* **2004**, *93* (17), 170802-4.
19
20
21
22 44. Chapel, J. P., Electrolyte Species-Dependent Hydration Forces between Silica
23 Surfaces. *Langmuir* **1994**, *10* (11), 4237-4243.
24
25
26
27 45. Kékicheff, P.; Marcelja, S.; Senden, T.; Shubin, V., Charge reversal seen in electrical
28 double layer interaction of surfaces immersed in 2: 1 calcium electrolyte. *J. Chem. Phys.*
29 **1993**, *99*, 6098-6113.
30
31
32
33 46. Pashley, R. M.; Israelachvili, J. N., Dlvo and hydration forces between mica surfaces
34 in Mg²⁺, Ca²⁺, Sr²⁺, and Ba²⁺ chloride solutions. *J. Colloid Interface Sci.* **1984**, *97* (2), 446-
35 455.
36
37
38
39 47. Schwartz, D. K., Langmuir-Blodgett film structure. *Surf. Sci. Rep.* **1997**, *27* (7-8),
40 245-334.
41
42
43
44 48. Ghaskadvi, R. S.; Carr, S.; Dennin, M., Effect of subphase Ca⁺⁺ ions on the
45 viscoelastic properties of Langmuir monolayers. *J. Chem. Phys.* **1999**, *111* (8), 3675-3678.
46
47
48
49 49. Miranda, P. B.; Du, Q.; Shen, Y. R., Interaction of water with a fatty acid Langmuir
50 film. *Chem. Phys. Lett.* **1998**, *286* (1-2), 1-8.
51
52
53
54
55
56
57
58
59
60

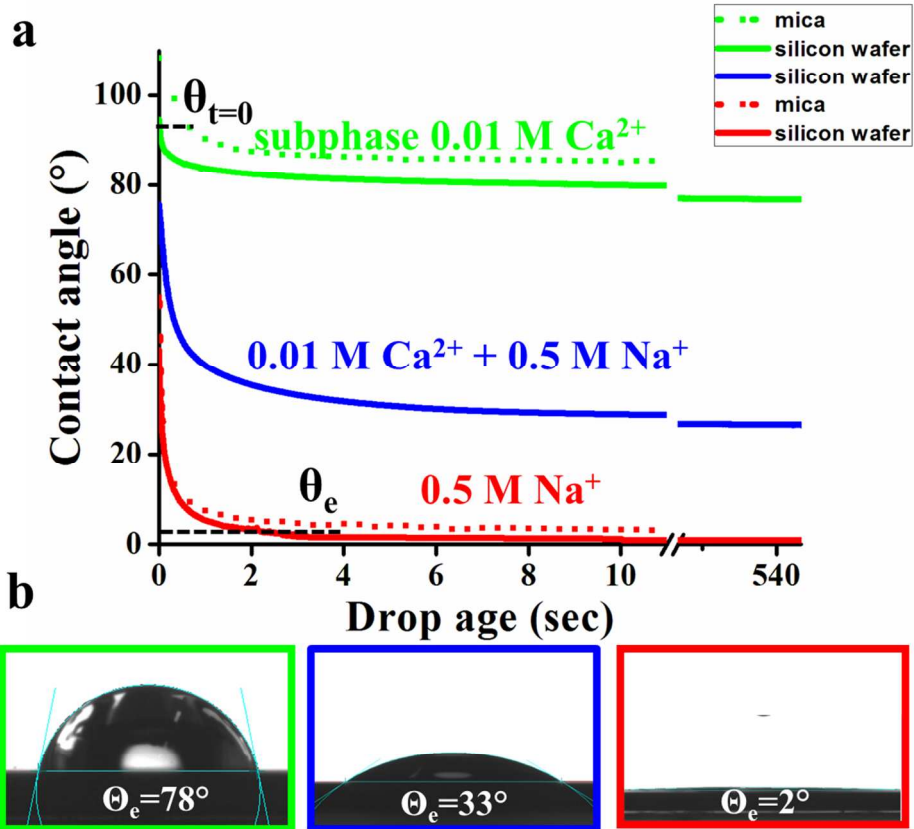
- 1
2
3 50. Le Calvez, E.; Blaudez, D.; Buffeteau, T.; Desbat, B., Effect of Cations on the
4 Dissociation of Arachidic Acid Monolayers on Water Studied by Polarization-Modulated
5 Infrared Reflection–Absorption Spectroscopy. *Langmuir* **2001**, *17* (3), 670-674.
6
7
8
9
10 51. Bloch, J. M.; Yun, W. B., Condensation of Monovalent and Divalent Metal-Ions on a
11 Langmuir Monolayer. *Phys. Rev. A* **1990**, *41* (2), 844-862.
12
13
14 52. June, D.; Franses, E. I., Interactions of Charged Langmuir Monolayers with Dissolved
15 Ions. *J. Chem. Phys.* **1991**, *95* (11), 8486-8493.
16
17
18 53. Diaz, M. E.; Cerro, R. L.; Montes, F. J.; Gala, M. A., Non-ideal adsorption of divalent
19 cations on a Langmuir monolayer: A theoretical model for predicting the composition of the
20 resulting Langmuir-Blodgett films. *Chem. Eng. J.* **2007**, *131* (1-3), 155-162.
21
22
23
24 54. Kovalchuk, V. I.; Zholkovskiy, E. K.; Bondarenko, M. P.; Starov, V. M.; Vollhardt,
25 D., Concentration polarization effect at the deposition of charged Langmuir monolayers. *Adv.*
26 *Colloid Interface Sci.* **2011**, *168* (1-2), 114-123.
27
28
29
30 55. Sobotka, H., Radioactive Tracer Studies of Monolayers. *J. Phys. Chem.* **1958**, *62* (5),
31 527-531.
32
33
34
35
36 56. Langmuir, I.; Schaefer, V. J., Composition of Fatty Acid Films on Water Containing
37 Calcium or Barium Salts. *J. Am. Chem. Soc.* **1936**, *58* (2), 284-287.
38
39
40 57. Dove, P. M.; Craven, C. M., Surface charge density on silica in alkali and alkaline
41 earth chloride electrolyte solutions. *Geochim. Cosmochim. Acta* **2005**, *69* (21), 4963-4970.
42
43
44
45 58. Mohwald, H., Phospholipid and Phospholipid-Protein Monolayers at the Air/Water
46 Interface. *Annu. Rev. Phys. Chem.* **1990**, *41*, 441-476.
47
48
49
50
51
52
53
54
55
56
57
58
59
60

Table of Contents Graphic:





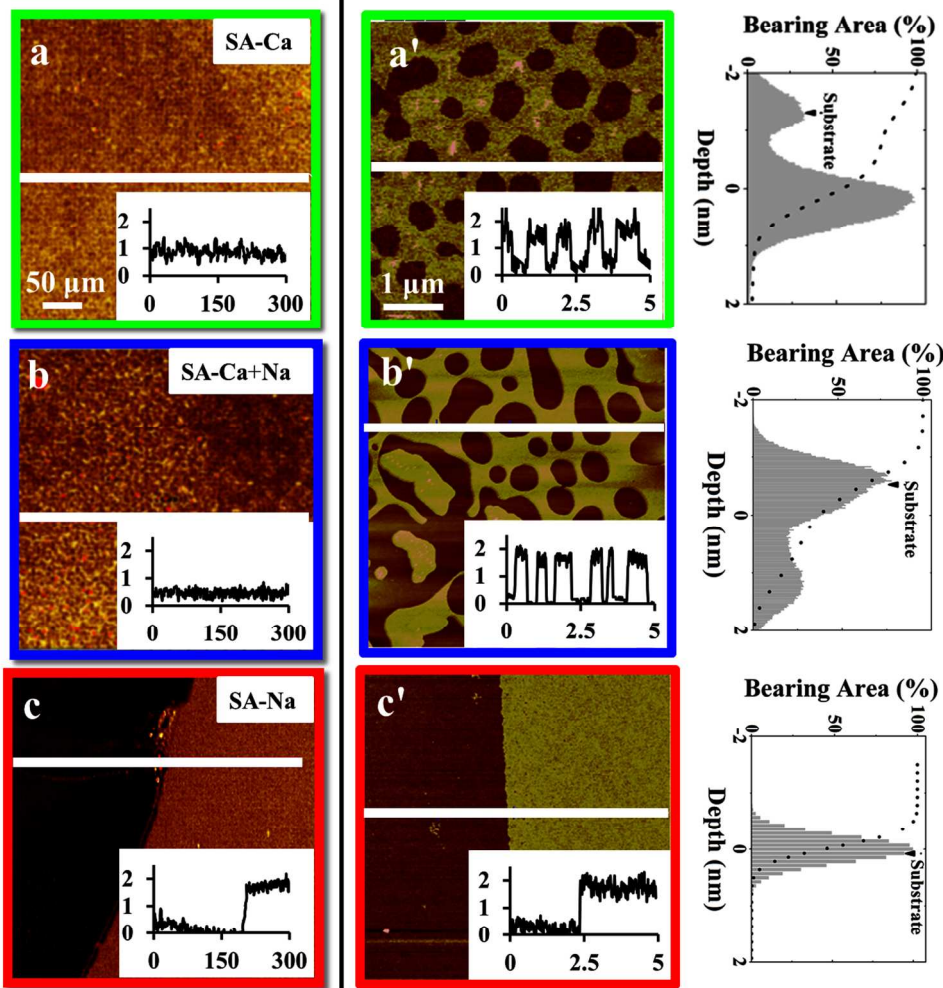
(a) Surface pressure versus area (π -A) isotherm of stearic acid with 0.5 M NaCl aqueous subphase. (a') Schematic illustration of deposited monolayer (b) AFM image (c) Ellipsometry thickness map and (d) corresponding profile of a SA-Na monolayer.
276x161mm (150 x 150 DPI)



(color online) Macroscopic wettability of three monolayers: SA-Ca (green), SA-Ca+Na (blue), and SA-Na (red). (a) Time evolution of the contact angle and (b) snapshots of drops in the final state showing the equilibrium contact angles (θ_e). Note: the axis break in (a) showing the final equilibrium angle. 201x176mm (150 x 150 DPI)

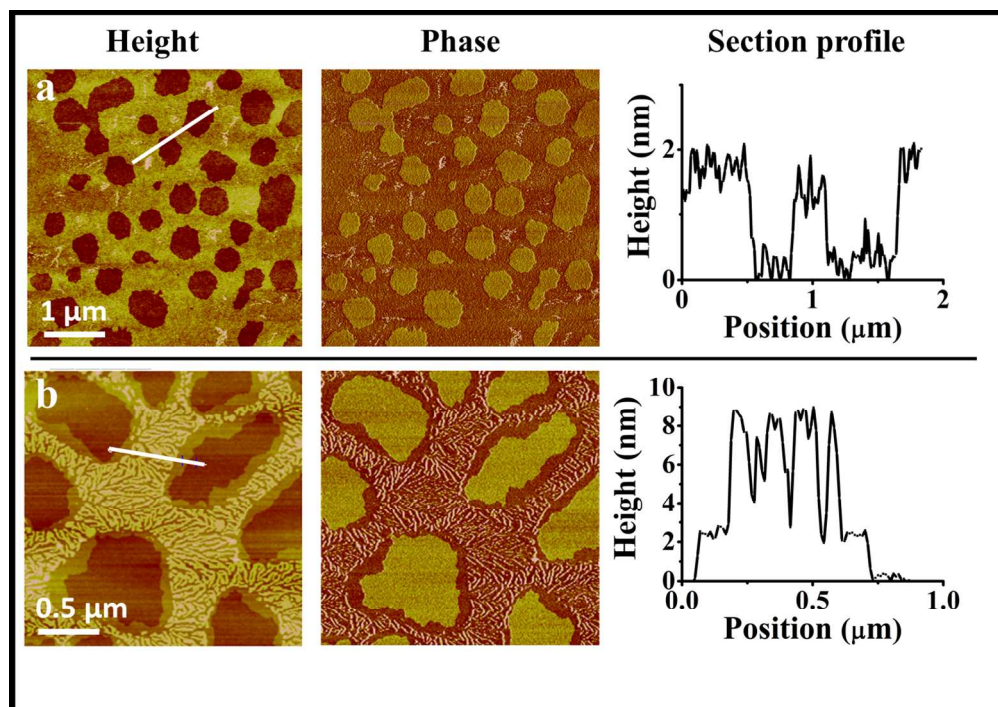
Ellipsometry

AFM

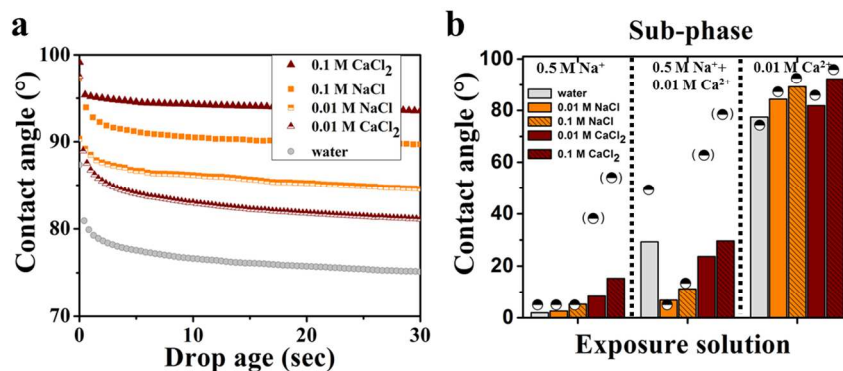


(color online) Macroscopic and microscopic images of SA-Ca (a and a'), SA-Ca+Na (b and b') and SA-Na monolayer (c and c') after exposure to water. a, b and c: imaging ellipsometry; a', b' and c': AFM). Inset images are height profiles corresponding to the white scan line (abscissa in μm; ordinate in nm). Histograms in a', b', and c' show the frequency and cumulative bearing area of the height levels.

233x280mm (150 x 150 DPI)



AFM height and phase images along with section profiles for (a) SA-Ca monolayer exposed to water and (b) SA-Ca+Na monolayer exposed to 0.01 M CaCl₂ solution. The different contrasts correspond to bare substrate, monolayer and multilayer.
261x183mm (150 x 150 DPI)



(a) Contact angle vs. time on SA-Ca monolayer for various compositions of exposure solution. (b) Equilibrium contact angles for all compositions of subphase and exposure solution (bars: experimental results from contact angle goniometry; symbols: values extracted from AFM images in combination with Cassie equation (see text for details).
246x104mm (150 x 150 DPI)

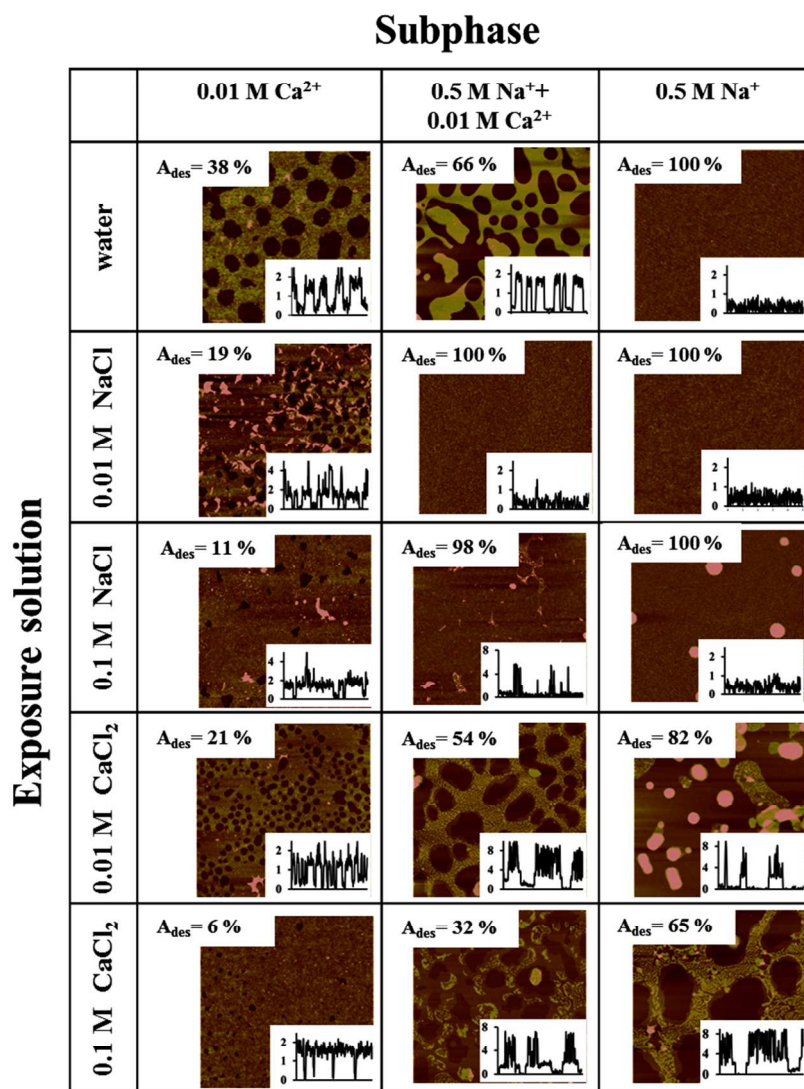
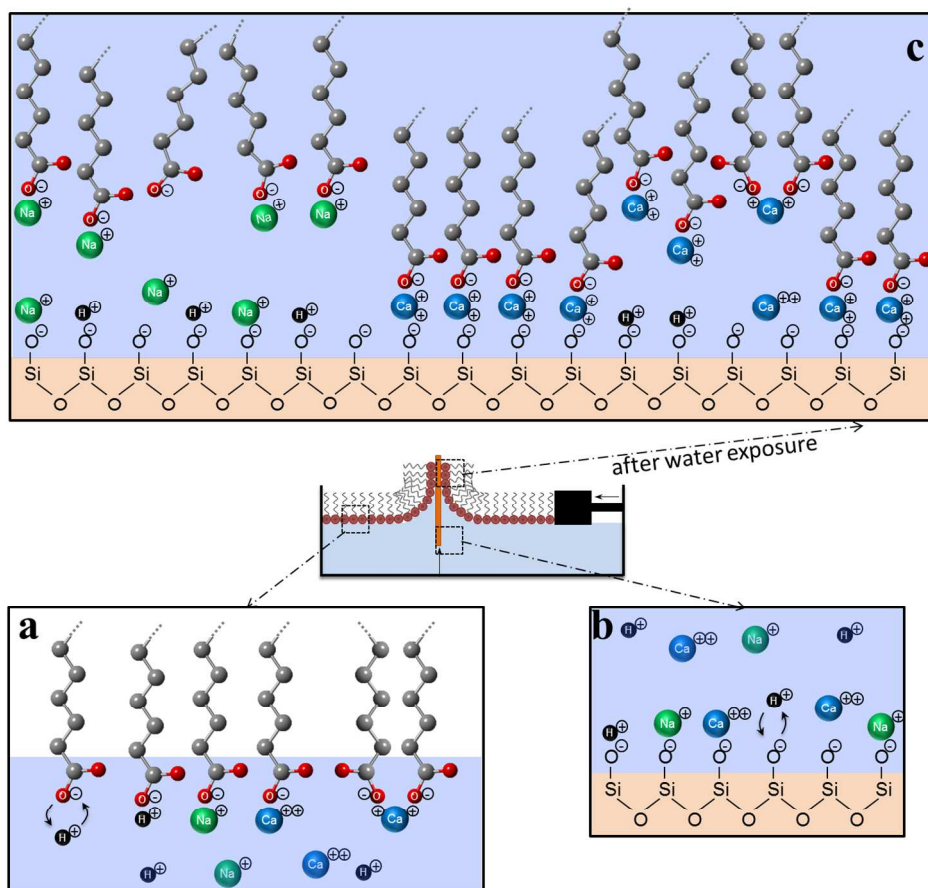


Figure 6. AFM viewgraphs of LB films prepared with all combinations of subphases after exposure to water and liquid compositions. Image size: $5 \times 5 \mu\text{m}^2$. Desorption area A_{des} indicates area fraction of exposed bare substrate. Insets show representative cross sections. Vertical scale: in nm. Horizontal scale: $5 \mu\text{m}$.
152x208mm (150 x 150 DPI)



Schematic illustration of monolayer adsorption-desorption process (a) formation of salt complexes with dissociated fatty acid at air-water interface (b) negatively charged substrate dipped under subphase (c) desorption of monolayer after water exposure.
260x237mm (150 x 150 DPI)

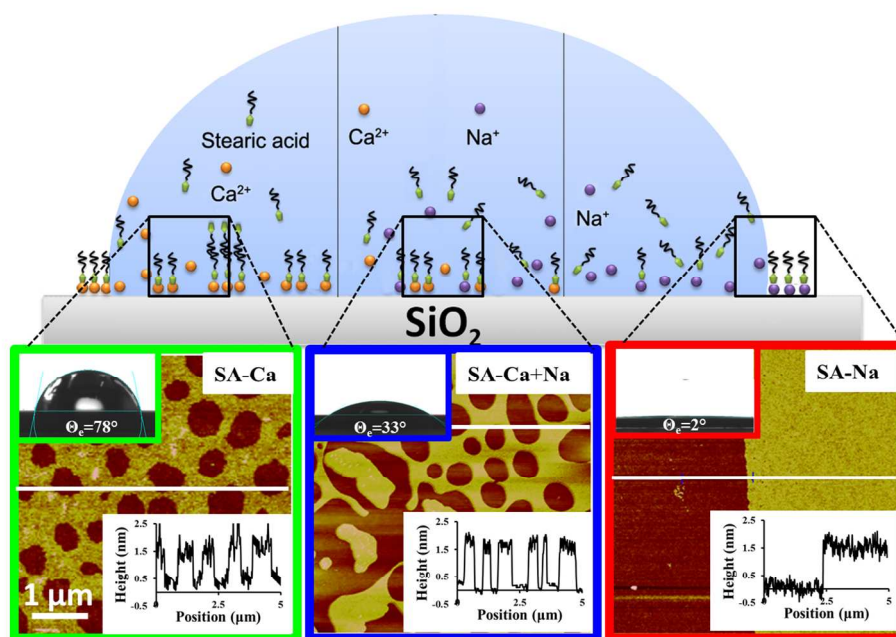


Table of Contents Graphic
249x175mm (150 x 150 DPI)